Target residues formed in the 4.4 GeV deuteron-induced reaction on gold

A. R. Balabekyan,[1] N. A. Demekhina,[2,3] G. S. Karapetyan,[4] D. R. Drnoyan,[5] V. I. Zhemenik,[5] J. Adam,[5] L. Zavorka,[5] A. A. Solnyshkin,[5] V. M. Tsoupko-Sitnikov,[5] J. Khushvaktov,[5] L. Karayan,[1] V. Guimarães,[4] A. Deppman,[4] and F. Garcia[6]

[1]*Yerevan State University, Alex Manoogian 1, Yerevan 0025, Armenia*

[2]*Yerevan Physics Institute, Alikhanyan Brothers 2, Yerevan 0036, Armenia*

[3]*Joint Institute for Nuclear Research (JINR), Flerov Laboratory of Nuclear Reactions (LNR), Joliot-Curie 6, Dubna 141980, Moscow Region, Russia*

[4]*Instituto de Fisica, Universidade de São Paulo, Rua do Matão, Travessa R 187, São Paulo, 05508-900 São Paulo, Brazil*

[5]*Joint Institute for Nuclear Research (JINR), Laboratory of Nuclear Problems (LNP), Joliot-Curie 6, Dubna 141980, Moscow Region, Russia*

[6]*Departamento de Ciências Exatas e Tecnológicas - DCET, Centro de Pesquisas em Ciência e Tecnologias das Radiações - CPqCTR, Universidade Estadual de Santa Cruz - UESC, Rodovia Jorge Amado km 16, Ilhéus, Buenos Aires, Brazil*

(Received 15 May 2014; revised manuscript received 10 September 2014; published 19 November 2014)

The production cross sections for 110 radioactive nuclides, with mass numbers $22 \leqslant A \leqslant 198$, were obtained from the interaction of 4.4 GeV deuteron with a ^{197}Au target using the induced-activity method. The deuteron beam was obtained from the Nuclotron of the Laboratory of High Energies (LHE), Joint Institute for Nuclear Research (JINR) at Dubna. Using the charge distribution data, we derived the total mass-yield distribution. The analysis of the mass-yield distribution allowed us to consider the coexistence of different channels in the interaction such as evaporation, fission, and multifragmentation.

DOI: 10.1103/PhysRevC.90.054612 PACS number(s): 25.45.−z, 25.60.Pj, 25.85.−w

I. INTRODUCTION

Many investigations in nuclear physics have been directed toward the understanding of the mechanism that drives the nucleus-nucleus interactions at energies of a few GeV per nucleon. From these investigations we can infer that the dependence of the nuclide formation cross sections upon the bombarding energy of the projectile (the excitation function) can be related to different reaction mechanisms. Thus, the question that always arise in these investigations is how to describe the projectile interaction with the target considering the several possible processes that can take place. In particular, a considerable amount of work has been devoted to the investigation of nuclide formation cross sections from reactions induced by different light projectiles on heavy targets, in various energy regimes [1–3]. The comparison of nuclide formation cross sections produced by different light projectiles on heavy targets can be very useful to emphasize the similarities and differences of such interactions in terms of possible reaction mechanisms involved. Several measurements, in a wide range of energy up to 300 GeV, have been performed for proton-induced reactions on a gold target, using different experimental methods (counter techniques and induced activity) to obtain the nuclide formation cross sections [3–10]. The main goal of such studies was the extraction of the properties of the different reaction channels from the analysis of a large amount of experimental cross sections (charge and mass distributions of the reaction products).

Another light particle probe used to investigate intermediate- to high-energy reactions is the deuteron. The particular interest in the deuteron-induced reactions on intermediate- to heavy-mass targets is due to the fact that the deuteron is considered to be the lightest weakly bound system, and hence, during the interaction with a target nucleus, the characteristics of the interactions of the individual nucleons can be derived. In particular, the reaction induced by high-energy deuterons can proceed with the deuteron either as whole nucleus or as noninteracting nucleons (proton plus neutron). The results of such investigations have been improving the theoretical models for reaction mechanisms. Experimental results of deuteron-induced reactions have also been of interest for accelerator technology and nuclear waste transmutation based on the accelerator-driven subcritical nuclear power reactors [11].

Nevertheless, a survey in the literature displays a considerable lack of experimental data for the deuteron interaction with a gold target. An experiment has been reported on the deuteron-induced reaction on a gold target at 2.1 GeV, where the cross sections for binary and ternary fission were measured by using plastic detectors [12]. Also Damdinsuren *et al.* [13] reported an investigation on the formation of evaporation residues from the interaction of 7.3 GeV deuterons with gold. However, this set of data was restricted to a small amount of reaction residues, which did not allow a complete analysis of the interaction. Another measurement was reported for target residues formed during the fission reactions of 4 GeV deuterons on gold [14]. In this work also limited information related only to the total fission cross section was reported, and they suggested that the total fission cross section of deuterons on ^{197}Au is the same, within the accuracy of the measurements, as for the fission induced by protons with the same total energy.

In the present paper we report the results for the mass and charge distributions of fragments produced by the interaction of a 4.4 GeV deuteron beam with a ^{197}Au target. This paper represents a sequel of the previous work [15], which was devoted to the investigation of the fragment kinematic features of the deuteron interaction with a gold target. The goal of the present work is to provide a set of experimental cross sections of residual nuclide formation. The experimental data obtained allowed us to consider the coexistence of different

reaction channels such as multifragmentation, evaporation, and fission processes. The determination of the cross sections for the formation of independent reaction residues and their corresponding integration over all fragment mass ranges allowed us to estimate the total reaction cross section. The comparison of the present results with the results reported for proton-induced reactions in the literature allows us to specify the role of the projectile in the reaction mechanism.

The present paper is divided as follows: Sec. II is devoted to give some details on the experimental procedure and data analysis. In Sec. III we present the results and the discussion, where we have performed a comparison of the results from the present deuteron-induced reaction with those from previous experiments of proton-induced reactions. Final conclusions are given in Sec. IV.

II. EXPERIMENTAL PROCEDURE

The 4.4 GeV deuteron beam was obtained from the Nuclotron of the Laboratory of High Energies (LHE), Joint Institute for Nuclear Research (JINR), Dubna, and used to irradiate a 39.13 mg/cm^2 thick gold target. The target consisted of a stack of 15 gold foils of 20×20 mm^2 in size. The total irradiation time was 28.6 hours with a total beam intensity integration of $(6.43 \pm 0.71) \times 10^{12}$ deuterons. The ^{27}Al$(d,3p2n)^{24}$Na reaction, with a known cross section of 14.2 ± 1.2 mb [13], was used to monitor the beam intensity. We have applied here the induced-activity method where the γ rays from the decay of the reaction residues formed in the target were measured, in an offline analysis. To detected the γ rays we have used high-purity germanium (HPGe) detectors with 28% relative efficiency and an energy resolution of 2 keV (^{60}Co at 1332 keV). The energy-dependent efficiency of the HpGe detectors was measured with standard calibration sources of ^{54}Mn, $^{57;60}$Co, ^{137}Cs, ^{154}Eu, ^{152}Eu, and ^{133}Ba. The γ spectra were evaluated with the code package DEIMOS32 [16]. The radioactive nuclei were identified by the energy and intensity of characteristic γ lines and by the respective half-lives of the nucleus. Nuclear properties, used for identification of observed isotopes, were taken from literature [17]. Measurements of the γ spectra started about 15 min after the completion of the irradiation and lasted for a year.

From the γ-ray spectra we obtained the individual cross section for 110 radioactive nuclides in the mass range $22 \leqslant A \leqslant 198$. The error in determining the cross sections depended on the following factors: the statistical significance of experimental results ($\leqslant$2–3%), the accuracy in measuring the target thickness and the accuracy of tabular data on nuclear constants ($\leqslant$3%), and the errors in determining the detector (energy-dependent) efficiency ($\leqslant$10%).

The fragment production cross sections are considered direct and independent (I) in the absence of a parent isotope contribution (which may give a contribution via $\beta^{\pm}$ decays) and are determined by the following equation:

$$\sigma = \frac{\Delta N\ \lambda}{N_d\, N_n\, k\, \epsilon\, \eta\, [1 - \exp(-\lambda t_1)] \exp(-\lambda t_2)[1 - \exp(-\lambda t_3)]}, \tag{1}$$

where σ is the cross section of the reaction fragment production (mb); ΔN is the yield (area under the photo-peak); N_d is the deuteron beam intensity (min^{-1}); N_n is the number of target nuclei (in 1/cm^2 units); t_1 is the irradiation time; t_2 is the time of exposure between the end of the irradiation and the beginning of the measurement; t_3 is the measurement time; λ is the decay constant (min^{-1}); η is the intensity of γ transitions; k is the total coefficient of γ-ray absorption in the target and in the detector materials, and ϵ is the γ-ray detection efficiency.

In the case where the cross section of a given isotope includes a contribution from the $\beta^{\pm}$ decay of neighboring unstable isobars, the cross section determination becomes more complicated [18] and is classified as cumulative (C). If the formation cross section of the parent isotope is known from experimental data, or if it can be estimated on the basis of other sources, the independent cross sections of daughter nuclei can be determined by the relation

$$\begin{aligned}\sigma_B = {} & \frac{\lambda_B}{[1 - \exp(-\lambda_B t_1)]\, \exp(-\lambda_B t_2)[\,1 - \exp(-\lambda_B t_3)]} \\ & \times \left[\frac{(\Delta N)_{AB}}{N_d\, N_n\, k\, \epsilon\, \eta} - \sigma_A\, f_{AB}\, \frac{\lambda_A\, \lambda_B}{\lambda_B - \lambda_A} \left(\frac{[1 - \exp(-\lambda_A t_1)]\, \exp(-\lambda_A t_2)\, [1 - \exp(-\lambda_A t_3)]}{\lambda_A^2} \right.\right. \\ & \left.\left. - \frac{[1 - \exp(-\lambda_B t_1)]\, \exp(-\lambda_B t_2)\, [1 - \exp(-\lambda_B t_3)]}{\lambda_B^2} \right) \right], \end{aligned} \tag{2}$$

where the subscripts A and B label the variables referring to the parent and the daughter nucleus, respectively; the coefficient f_{AB} specifies the fraction of A nuclei decaying to B nucleus ($f_{AB} = 1$, when the contribution from the β decay corresponds to 100%), and $(\Delta N)_{AB}$ is the total photo-peak yield associated with the decays of the daughter and parent isotopes. The effect of the precursor can be negligible in some limiting cases: where the half-life of the parent nucleus is very long, or in the case where its contribution is very small. The induced-activity method imposes a severe restriction for the measurement of some the reaction products. For example, it is impossible to measure stable or very long-lived isotopes and very short-lived isotopes.

III. RESULTS AND DISCUSSION

The experimental cross sections for the reaction fragment production in the mass range of $22 \leqslant A \leqslant 198$ are presented in Table I. In this table, the type of cross sections [independent (I) or cumulative (C)] is present as well as the corresponding type

TABLE I. The cross sections of fragments formed by the reaction of 4.4 GeV deuterons with ^{197}Au. Independent cross sections are indicated by (I) and the cumulative cross section by (C).

Element	Reac. (decay)	σ (mb)
^{24}Na	C (β^-)	8.02 ± 0.80
^{28}Mg	C (β^-)	2.30 ± 0.66
^{42}K	C (β^-)	3.34 ± 0.13
^{43}K	C (β^-)	5.0 ± 1.7
^{47}Ca	C (β^-)	0.70 ± 0.16
^{44}Sc	I (β^+)	1.76 ± 0.70
^{44m}Sc	I (β^+)	0.45 ± 0.16
^{46}Sc	I (β^-)	4.05 ± 0.46
^{48}Sc	I (β^-)	1.71 ± 0.71
^{48}V	C (β^+)	1.14 ± 0.09
^{52}Mn	C (β^+)	0.66 ± 0.09
^{54}Mn	I (β^+)	3.59 ± 0.69
^{59}Fe	C (β^-)	1.81 ± 0.36
^{55}Co	C (β^+)	2.26 ± 0.72
^{56}Co	C (β^+)	0.34 ± 0.10
^{58}Co	I (β^+)	3.77 ± 0.15
^{60}Co	C (β^-)	3.22 ± 0.47
^{65}Zn	C (β^+)	4.29 ± 0.33
^{72}Zn	C (β^-)	0.16 ± 0.09
^{71}As	C (β^+)	0.30 ± 0.04
^{72}As	C (β^+)	3.40 ± 0.22
^{74}As	I (β^+)	3.02 ± 0.24
^{75}Se	C (β^+)	4.82 ± 0.12
^{77}Br	C (β^+)	2.18 ± 0.42
^{82}Br	I (β^-)	1.68 ± 0.05
^{81}Rb	C (β^+)	5.92 ± 0.66
^{83}Rb	I (β^+)	7.17 ± 0.90
^{84}Rb	I (β^+)	3.20 ± 0.30
^{83}Sr	C (β^+)	4.04 ± 0.07
^{85}Sr	C (β^+)	10.3 ± 2.1
^{86}Y	C (β^+)	6.21 ± 0.88
^{87}Y	C (β^+)	8.93 ± 1.02
^{88}Y	C (β^+)	6.01 ± 0.80
^{88}Zr	C (β^+)	9.44 ± 0.50
^{89}Zr	C (β^+)	7.26 ± 0.90
^{95}Zr	C (β^-)	0.7 ± 0.38
^{90}Nb	C (β^+)	4.80 ± 0.94
^{92m}Nb	I (β^+,β^-)	0.38 ± 0.04
^{95}Nb	I (β^-)	1.09 ± 0.30
^{95m}Nb	C (β^-)	0.35 ± 0.03
^{93}Tc	C (β^+)	3.46 ± 0.42
^{94}Tc	C (β^+)	2.67 ± 0.34
^{96}Tc	I (β^+)	2.25 ± 0.30
^{103}Ru	C (β^-)	1.32 ± 0.13
^{99}Rh	C (β^+)	4.92 ± 0.07
^{100}Rh	I (β^+)	2.13 ± 0.12
^{102}Rh	I (β^+,β^-)	3.85 ± 0.60
^{102m}Rh	I (β^+,β^-)	13.4 ± 1.5
^{117m}Sn	C (IT)	0.23 ± 0.02
^{124}Sb	I (β^-)	2.80 ± 0.60
^{126}Sb	C (β^-)	2.40 ± 0.46
^{119}Te	C (β^+)	0.66 ± 0.09
^{132}Te	C (β^-)	2.93 ± 0.88
^{124}I	I (β^+)	0.46 ± 0.03
^{126}I	I (EC,β^-)	2.02 ± 0.34
^{133}I	C (β^-)	1.22 ± 0.16
^{127}Xe	C (β^+)	10.9 ± 1.2
^{131}Ba	C (β^+)	14.9 ± 1.2
^{140}Ba	C (β^-)	0.79 ± 0.08
^{139}Ce	C (β^+)	11.71 ± 0.95
^{143}Ce	C (β^-)	7.4 ± 1.6
^{143}Pm	C (β^-)	12.94 ± 0.96
^{144}Pm	C (β^+)	1.54 ± 0.14
^{148m}Pm	I (β^-)	1.10 ± 0.29
^{145}Eu	C (β^+)	14.3 ± 2.0
^{146}Eu	I (β^+)	18.1 ± 1.8
^{147}Eu	I (β^+)	34.0 ± 3.0
^{148}Eu	I (β^+)	1.09 ± 0.17
^{149}Eu	C (β^+)	19.2 ± 1.4
^{146}Gd	C (β^+)	13.2 ± 2.1
^{147}Gd	I (β^+)	6.2 ± 1.2
^{149}Gd	I (β^+)	17.86 ± 0.58
^{153}Gd	I (β^+)	9.70 ± 0.90
^{147}Tb	C (β^+)	2.99 ± 0.50
^{149}Tb	C (β^+)	5.39 ± 0.97
^{153}Tb	C (β^+)	4.01 ± 0.97
^{160}Tb	I (β^-)	8.94 ± 0.80
^{167}Tm	C (β^+,β^+)	21.8 ± 3.2
^{168}Tm	I (β^+,β^-)	2.62 ± 0.18
^{171}Lu	C (β^+)	26.8 ± 3.0
^{172}Lu	C (β^+)	4.16 ± 0.42
^{173}Lu	C (β^+)	25.2 ± 1.8
^{177m}Lu	C (β^-)	1.36 ± 0.30
^{175}Hf	C (β^+)	27.1 ± 3.0
^{181}Hf	C (β^-)	2.41 ± 0.24
^{182}Ta	C (β^-)	2.75 ± 0.75
^{182}Re	C (β^+)	49.0 ± 9.4
^{184g}Re	I (β^+)	0.92 ± 0.18
^{184m}Re	I (β^+)	4.09 ± 0.25
^{185}Os	I (β^+)	29.0 ± 5.4
^{185}Ir	C (β^+)	26.9 ± 2.2
^{190}Ir	I (β^+)	4.09 ± 0.80
^{192}Ir	I (EC,β^-)	3.12 ± 0.70
^{194m}Ir	C (β^-)	1.13 ± 0.10
^{188}Pt	C (β^+)	27.4 ± 8.0
^{191}Pt	C (β^+)	15.0 ± 3.5
^{100}Pd	C (β^+)	1.31 ± 0.36
^{105}Ag	C (β^+)	8.1 ± 1.1
^{106m}Ag	I (β^+,β^-)	2.31 ± 0.40
^{110m}Ag	I (β^+,β^-)	0.32 ± 0.02
^{111}In	C (β^+)	8.0 ± 1.1
^{113}Sn	C (β^+)	17.4 ± 1.9
^{194}Au	C (β^+)	26.6 ± 2.0
^{195}Au	C (β^+)	15.4 ± 2.6
^{196}Au	I (β^+,β^-)	140 ± 13
^{198g}Au	I (β^-)	1.56 ± 0.25
^{198m}Au	I(β^-)	7.41 ± 0.50

of decay, β^- or β^+. As one can see from the Table I, most of residuals are nuclei decaying by β^+. This can be connected to the fact that the average multiplicity of the emitted neutrons is a

few times higher than the average proton emission multiplicity in this nuclear reaction [19].

As can be seen in from Table I, the highest production cross section was obtained for the ^{196}Au residue. Residues such as ^{196}Au and ^{198}Au can be formed by a one-neutron transfer (stripping or pickup) reaction. It can be seen from Table I that the probability of ^{196}Au production (neutron stripping) is several times higher than that of the neutron pickup transfer reaction or any other process leading to the formation of ^{198}Au. This can be explained by the fact that the neutron interaction in the deuteron-nucleus reaction, in the energy range of about GeV, is larger than the proton-nucleus interaction [19]. The inelastic cross section for neutron-nucleus reactions, in the energy range of several GeV, is about 1–2 b [20]. Thus, the $(n,2n)$ stripping reaction can give a significant contribution to the ^{197}Au$(d,X)^{196}$Au reaction and it can be, indeed, responsible for increasing the cross section for the production of the ^{196}Au nuclide.

Using the production cross sections of the individual fragments we can construct the mass distribution (cross section of each isobar as a function of the mass number A). However, to obtain the cross section for each isobar it is necessary to estimate the cross sections of the isotopes not measured by the induced-activity method. The cross sections for these fragments can be obtained from the analysis of the charge distribution of the corresponding isobar chain, i.e., the cross section as a function of Z for a given A. The charge distribution for each isobar can be constructed by using the independent cross sections of the reaction residues. In the present work the charge distribution of each isobar chain was analyzed with the expression from Ref. [3]:

$$\sigma(Z,A) = \sigma(A)\exp(-R|Z - SA + TA^2|^{3/2}), \qquad (3)$$

where $\sigma(Z,A)$ is the independent cross section for a given nuclide with atomic charge Z and mass number A; $\sigma(A)$ is the total isobaric cross section of the mass A. The parameter R defines the width of the charge distribution, while the parameters S and T define the most probable charge (Z_p) for a given isobar chain A. These parameters were obtained by fitting the cross section data of fragments from the mass region $A = 40$ to $A = 200$. To uniquely specify the variables R, S, and T, it is necessary to consider more than four independent yield cross sections for each isobar. In case of shortage of the experimental data with independent cross section, for a given isobar chain, we used the similarity of charge distribution curves of the isobaric chains [21,22]. However, at first, only independent cross sections (I) were used in the fitting of the charge distributions. Hence, during the successive approximation procedures, the estimation of the independent component of the cumulative cross section could be extracted.

During the fitting procedure it was found that the values of the R and S parameters were constant for all mass ranges of the reaction products, but the parameter T was larger for the spallation fragments. This means that the width of the charge distribution for a given mass number (isobar) is about the same for all ranges of product mass number. The values for R and S obtained from the fitting procedure were $R = 30A^{-0.79}$ and $S = 0.47$. The parameter $T = 2.3 \times 10^{-4}$ was used for the mass range of $40 \leqslant A \leqslant 130$ while $T = 3.2 \times 10^{-4}$ had to be used for the spallation-evaporation mass range ($A > 130$). The parameters for the mass range $40 \leqslant A \leqslant 130$ are in good agreement with those for the 7.3 GeV $d + ^{181}$Ta system ($S = 0.477$ and $T = 2.4 \times 10^{-4}$) from Ref. [23]. This result can confirm that the charge distributions of the fragments are mainly determined by the properties of reaction residues and not by the way they were formed. It is also well known that the isotope distributions are largely independent of the original nucleus; their position, shape, and width depend only on the fragment mass number [24].

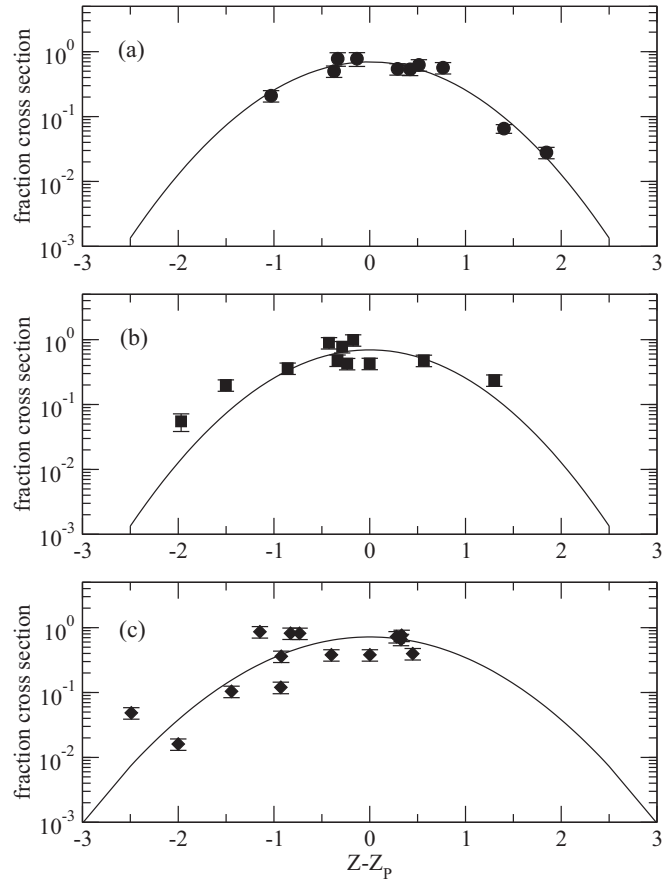

FIG. 1. The charge distributions for the isobaric chains in the mass ranges (a) $A = 42$–65, (b) $A = 83$–127, (c) $A = 133$–198 for the 4.4 GeV deuteron-induced reaction on ^{197}Au. The solid line is the result of the fitting procedure explained in the text.

The charge distributions for some of the isobar chains can be seen in Figs. 1(a)–1(c). In these figures we show the fractional cross section (the ratio of fragment production cross section to the total cross section for the given mass number) as a function of the charge difference $(Z_p - Z)$, for different mass ranges. The corresponding calculated Gaussian charge distribution, using the parameters R, S, and T as discussed above, are also shown. This is an indication that the charge difference $(Z - Z_p)$ moves toward the more neutron-deficient nuclei for mass chains lighter than $A > 130$, where more neutron-rich nuclei are preferable formed. This effect can be clearly seen in Fig. 2, where we present the dependence of the average atomic

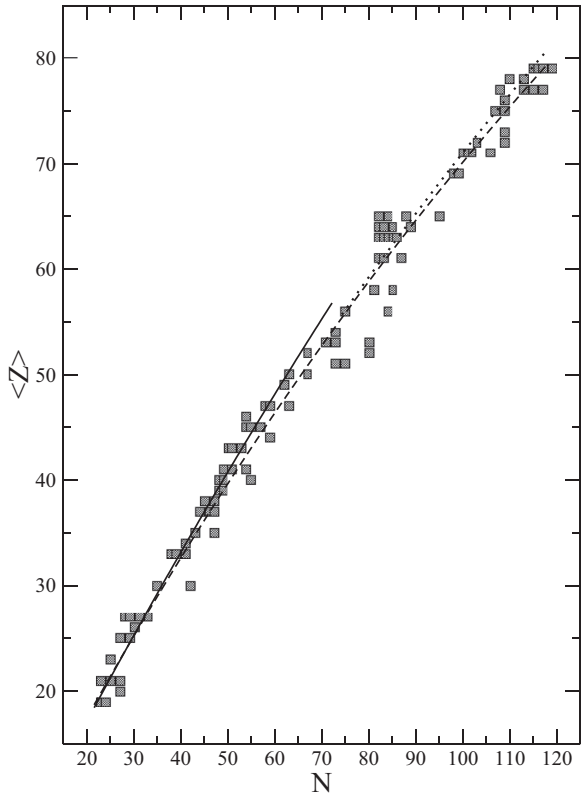

FIG. 2. Average atomic number as a function of neutron number for the observed nuclides. The black dashed line corresponds to the stable nuclei, the black solid line is for Z_p for $A < 130$, and the dotted line is for Z_p for $A > 130$.

number as a function of neutron number for the observed nuclides in our experiment. In the figure the dashed solid line corresponds to stable nuclei, the black solid line is Z_p for $A < 130$, and the dotted line is Z_p for $A > 130$. We can clearly see in Fig. 2 the displacement between Z_p and stable Z. The appreciable effect is an overall tiny displacement towards the neutron-poor side due to evaporation, also indicating that the (neutron rich) contribution from fission is small. In the frame of the intranuclear cascade model, an intermediate nuclear state with high excitation energies results in a large number of evaporated nucleons. Hence, as a result of the evaporation, fragmentation, and fission process, a set of neutron-deficient nuclei are expected to be formed, as can be observed in the present work. A similar situation was observed in the works of Refs. [25] and [26]. We can conclude that the displacement of the charge distribution curves for residuals with $A < 130$ toward the neutron-deficient nuclei can be a result of the contribution from the higher excited after-cascade nuclear states. An interesting feature of these distributions is that the width parameter (R) obtained is the same as the ones obtained for the 1.0–3.0 GeV proton + ^{197}Au system [3].

A higher excitation energy would correspond to an increase in the neutron emission, which in turn would result in a larger contribution of neutron-deficient composite systems, as well as an increase in the number of neutron evaporations from the reaction residues. In our experiment low-energy

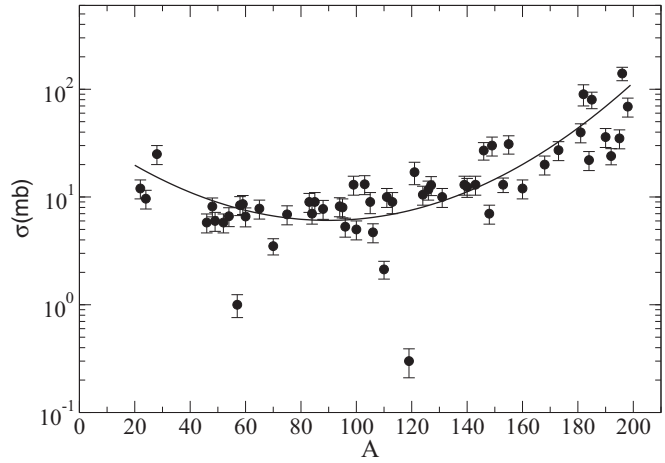

FIG. 3. Mass-yield distribution of the isobars produced by the 4.4 GeV deuteron-induced reaction on ^{197}Au. The solid line shows the general trend of the isobaric cross sections of the reaction fragments.

excited residues with mass number $A > 130$ and residues with $A < 130$ but with higher excitation energy are being produced. This fact is confirmed by our recent study of the kinematics properties of the reaction residues [15]. Similar behavior was observed for fission induced by different probes such as protons and neutrons on ^{238}U and ^{232}Th [21,27,28], indicating that the charge distributions are determined more by the excitation energy and nuclear properties of the reaction products than by the choice of the projectile or the reaction channel.

By integrating the charge distribution with the use of Eq. (3) we could derive the isobaric cross sections [$\sigma(A)$] for each mass number. These cross sections as a function of the mass number A is called the mass-yield distribution. The mass-yield distribution obtained in the present work is shown in Fig. 3. The smooth curve in the figure corresponds to a fifth-degree polynomial fit for the mass range $22 \leqslant A \leqslant 198$, which corresponds to the inclusion of contributions from different processes such as evaporation, fission, and multifragmentation. The analysis of the mass-yield distribution present in Fig. 3 is based on the fact that we should consider the coexistence of different mechanisms for the fragment formation. For clarity, it should be mentioned that for this high-energy nuclear reaction, the residues can be produced by several process: evaporation, fission, and multifragmentation.

By analyzing the experimental mass distribution one can observe a sharp increase in the cross section for the fragments very close to the target. The fragment with the masses $A > 130$ is connected to the spallation-evaporation process during the cooling mechanism of the cascade remnant. Reaction residues in this mass range have a decreasing cross section with the increase of the number of the emitted nucleons. The production of fragments in the mass range $A = 120$–150 can be interpreted as a transition from the spallation-evaporation mechanism to fission and multifragmentation, where the fraction of the competing processes varies with the mass of the cold residue. The reaction residues in the mass range of $40 \leqslant A \leqslant 120$ can be attributed to the fission and

multifragmentation processes. For this mass range, the energy transferred to the after cascade remnants promotes the opening of new reaction channels, which includes multifragmentation. As it was shown in the work of Napolitani *et al.* [29], in the vicinity of multifragmentation threshold, both fission and multifragmentation processes can contribute to the formation of the residue in this mass range. Finally, the production of light fragments with masses smaller than $A = 40$ are from asymmetric fission and from multifragmentation in connection with the liquid-gas phase transition [30,31].

Integration of the mass-yield curve over mass number range $40 \leqslant A \leqslant 198$ gives a total cross section for the production of target residues equal to 2.20 ± 0.44 b. We have chosen the lower limit of $A = 40$ mass because the multiplicity for the smaller mass fragments is unknown. These lower mass reaction residues could have been formed by an interaction where another heavy fragment had survived and had already been accounted for.

Part of the total production cross section in this experiment can be attributed to the fission contribution. The mass distribution of fission fragments is expected to be symmetric for this system as confirmed by the results of the GSI experiment on $d + {}^{197}$Au in inverse kinematics [32]. In the present case, due to the inclusive measurement, such a contribution would be expected as a bump in the mass range of $50 \leqslant A \leqslant 120$ above the spallation data. However, by analyzing the isobaric cross sections of the mass-yield distribution in Fig. 2 we can conclude that fission has a small contribution in the present reaction.

A semiempirical approach for the fission probability of proton-induced fission on targets from $^{\text{nat}}$Ag to ^{239}Pu nuclei, in a wide range of energy (several tens of MeV to 3 GeV) has been proposed by Fukahori [33]. From this model we can determined the fissility, which is defined as the ratio of the total fission cross sections to the total reaction cross sections. Thus, according to this proposed approach, the fissility for ^{197}Au increases from 0.3% at an excitation energy of 100 MeV to a saturation of 5% at 300 MeV excitation energy. For the 2.1 GeV deuteron-induced fission experiment, a fissility of 5% was obtained [12], in agreement with the more recent results by Stoulos *et al.* [14] which gives 4–10% of the total reaction cross section. The constant fission cross section for high-energy deuterons (in the GeV energy regime) would be a clear indication that contributions of competing processes, such as the emission of nucleons and heavier particles, at the preequilibrium and equilibrium phases of the interaction, start playing an important role.

A. Energy and momentum transfer

We applied the hard sphere model [34] for nucleus-nuclear interactions to obtain the impact parameter of the collision. In this model, the interacting nuclei are related to the overlap of the two sharp spheres formed during the collision and the total reaction cross section is given in terms of the two-parameter expression:

$$\sigma_R = \pi r_0^2 \left(A_T^{1/3} + A_P^{1/3} - b_{Tp}\right)^2 \text{ fm}^2, \tag{4}$$

where A_T and A_P are the mass numbers of the target and projectile nuclei, respectively; r_0 is the reduced radius ($R_i = r_0 A_i^{1/3}$) and b_{Tp} is the overlap parameter.

The parameter $b_{Tp} = 0.97$ fm was estimated for the present work by putting the experimentally determined value of the total reaction cross section in Eq. (4). Using this value for b_{Tp} we can also determine the impact parameter b by using the following relation:

$$b = r_0 \left(A_T^{1/3} + A_P^{1/3} - b_{Tp}\right) \text{ fm}. \tag{5}$$

The average impact parameter obtained for the present work is $b = 8.37$ fm. This value is larger than $b = 7.45$ fm obtained for the same system at 7.3 GeV [13], which can indicate a more peripheral interaction in our case.

Considering the small binding energy of the deuteron and the large impact parameter obtained in the present work, one can also suggest that mainly only one of the nucleons (proton or neutron) of the deuteron interacts with the nucleus, the other being just a spectator. This assumption has been confirmed by the theoretical work of Ref. [19]. The pattern of the mass distribution shown in Fig. 2 indicates that the main portion of the reaction cross section might come from the evaporation-residue production, which should have low excitation energy and low linear momentum transfer, as clearly observed in the previous paper on the kinematics characteristics of fragments from the $d + {}^{197}$Au reaction [15]. As mentioned before, evaporation-residue production would correspond to fragments with mass close to that of the target with low linear momentum and excitation energy, which in turn could be associated with a large impact parameter. A more central collision, with low impact parameters, would be responsible for the formation of high-excitation remnants from some other mechanisms such as fission or multifragmentation. The linear momentum transfer, being a decreasing function of the impact parameter, could also be related to the number of emitted nucleons (which is proportional to the excitation energy). This fact would also explain the peripheral characteristic of the present high-energy deuteron-induced reaction.

Regarding the energy transfer mechanism, it is interesting to compare our data with similar data from high-energy proton- and deuteron-induced reactions. In Figs. 4(a) and 4(b) we have performed such a comparison by plotting the ratio of the cross section of residuals from the 4.4 GeV deuteron on ^{197}Au of the present work and the corresponding cross sections of residuals from the 3.65 GeV [8] and 3.0 GeV [3] proton-induced reactions on ^{197}Au, respectively. As one can see in the figure, the cross sections for the heavier mass fragments (fragments formed by the evaporation-residue production process) are similar for proton- and deuteron-induced reactions. Formation of these nuclides would correspond to a peripheral collision with large impact parameter and low excitation energy. On the other hand, as one can see in Fig. 4(b), even with close incident energies, the use of a deuteron projectile instead of a proton has a remarkable effect of enhancing the cross section for the mass region $A = 20$ to 110. The mass region of $A = 20$–60 is predominantly due to the multifragmentation process, while the region $A = 90$–110 fills of the gap between fission fragments and evaporation residues, where the fraction

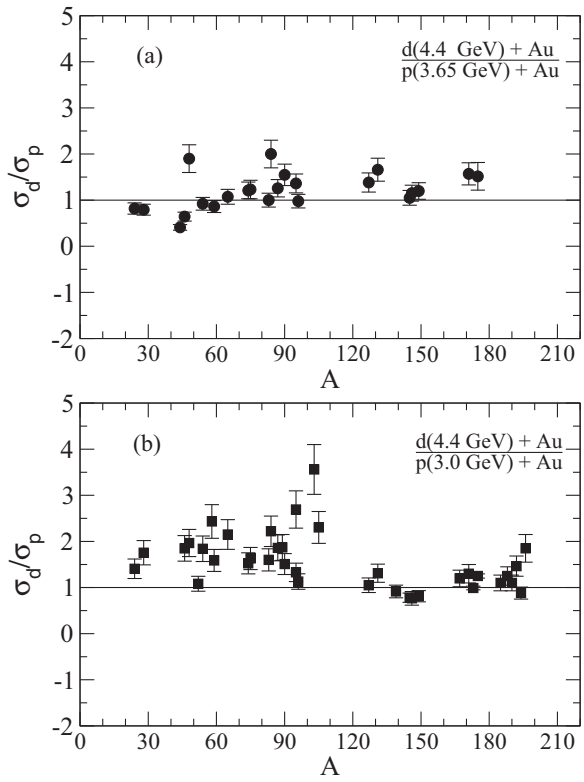

FIG. 4. The ratio of experimental cross sections, σ_d/σ_p, obtained for the residues from the 4.4 GeV deuteron reaction on ^{197}Au target of the present work and (a) from the 3.65 GeV proton-induced reaction on ^{197}Au from Ref. [8] and (b) from the 3.0 GeV proton-induced reaction on ^{197}Au from Ref. [3].

of the competing processes varies with the mass of the cold residue. A similar effect was pointed out in Ref. [32] for deuteron- and proton-induced reactions on a lead target. The prominent discrepancy in Fig. 3(b) can be explained as being due to the effect of changing the mechanism: a depletion of spallation-evaporation production is compensated by a larger production from the multifragmentation process ($A < 60$), which is more relevant for higher energy incident protons [29,35]. We also compared our 4.4 GeV deuteron-induced reaction results with those from the 7.3 GeV deuteron-induced reaction on the same gold target [13]. The cross section ratios of residues are shown in Fig. 5, which shows almost the same effect as in Fig. 4(b), except for the cross section ratio for ^{196}Au, which, as already mentioned, can be formed by the one-neutron transfer reaction.

By considering the intranuclear cascade (INC) + evaporation model and the cooling process applied to the spallation reactions, Cugnon *et al.* [19] calculated the mean multiplicity of emitted particles (neutrons, protons, and other charged particles) for deuteron-, proton-, and neutron-induced reactions on a gold target at the same energy. The values of the neutron multiplicity are $\langle n\rangle = 31(3)$ for the $d + ^{197}$Au reaction, $\langle n\rangle = 21(2)$ for $p + ^{197}$Au, and $\langle n\rangle = 21(2)$ for the $n + ^{197}$Au reaction at the energy 2.2 A GeV. As we can see, the total neutron multiplicity in deuteron-induced reactions is less than the sum of the neutron multiplicities

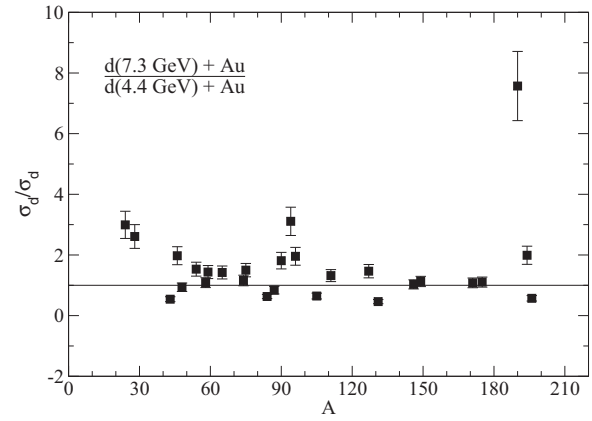

FIG. 5. The ratio of experimental cross sections σ_d/σ_d of residues from the reactions of 7.3 GeV deuterons [13] and the data of the present work of 4.4 GeV deuterons on the same ^{197}Au target.

in proton- and neutron-induced reactions, for the same target and at the same incident energy per nucleon. Moreover, the ratio of multiplicities of emitted particles for the deuteron- and proton-induced reactions is 1.5 ± 0.2. This value should correspond, on average, to the cross section ratio of the reaction residue formation, and, as it can be seen, it is in satisfactory agreement with our experimental results.

The non-additivity of the neutron and proton in the deuteron projectile can be confirmed by considering the ratio of the cross section of residuals from the present work and the corresponding cross sections of residuals from the 3.65 GeV [8] and 3.0 GeV [3] proton-induced reactions (Fig. 4, σ_d/σ_p): 1.2 ± 0.2 and 1.5 ± 0.2, respectively. This fact reasonably indicates a more peripheral character of the present deuteron collision, and the fact that one of the nucleons from the deuteron may not interact at all with the target, remaining as spectator.

IV. CONCLUSION

The production cross sections for more than 100 radioactive products formed in the 4.4 GeV deuteron-induced reaction with ^{197}Au target have been measured. The charge distributions were analyzed in the terms of a three-parameter equation. It was found that the width of these charge distributions for a given mass number is the same for all ranges of mass number of the reaction residues, but the the charge difference $(Z - Z_p)$ is smaller for the lighter mass chains. The mass-yield distribution of target residues could be constructed from the determined isobaric cross sections for fragments with $A > 40$. It was suggested that a few sources having different excitation energies can take part in the formation of reaction residues. The mass distribution also indicates contribution of different processes, such as evaporation, fission, and multifragmentation, for the formation of the residues.

The ratio of the experimental cross sections of proton- and deuteron-induced reactions is in a good agreement with the ratio of theoretical calculations for the multiplicity of the emitted particles in the cascade and cooling stages.

From the data of the present work, one may clearly see that the ratio of cross sections between deuteron- and proton-induced reactions is comparable when considering the residue production (which dominates the total cross section), reinforcing the idea that the reaction has a peripheral character. However, there is a sizable difference when one considers the intermediate-mass fragment production. The difference in cross section for this mass region may indicate that when the collision is more central, the deuteron is more effective in inducing multifragmentation. The mechanism of interaction of the deuteron with the nucleus is not provided by the additional interaction of two nucleons in the deuteron. The deuteron, as a weakly bound nucleus, can disintegrate and exhibit a one-nucleon collision character in most cases of reactions with high impact parameter.

ACKNOWLEDGMENT

G.K. is grateful to Fundação de Amparo à Pesquisa do Estado de São Paulo (FAPESP) for Grants No. 2011/00314-0 and No. 2014/00284-1, and also for support from the International Centre for Theoretical Physics (ICTP) under the Associate Grant Scheme. The authors are grateful to Dr. S. Avdeev of LNP JINR for enabling this experiment, and also to Kh. Abraamyan of LHEP JINR for help during the experiment.

[1] X. Ledoux *et al.*, Phys. Rev. C **57**, 2375 (1998).
[2] A. Ingemarsson, J. Nyberg, P. U. Renberg *et al.*, Nucl. Phys. A **676**, 3 (2000).
[3] S. B. Kaufman and E. P. Steinberg, Phys. Rev. C **22**, 167 (1980).
[4] R. Michel, R. Bodemann, H. Busemann *et al.*, Nucl. Instrum. Methods B **129**, 153 (1997).
[5] S. B. Kaufman, M. W. Weisfield, E. P. Steinberg *et al.*, Phys. Rev. C **14**, 1121 (1976).
[6] A. Letourneau, A. Böhm, J. Galin *et al.*, Nucl. Phys. A **712**, 133 (2002).
[7] S. R. Hashemi-Nezhad, I. Zhuk, A. Potapenko, W. Westmeier, and R. Brandt, Nucl. Instrum. Methods A **679**, 82 (2012).
[8] P. Kozma and C. Damdinsuren, Czech. J. Phys. B **40**, 38 (1990).
[9] J. Gindler, H. Monzel, J. Buschmann *et al.*, Nucl. Phys. A **145**, 337 (1970).
[10] D. J. Morrissey, W. Loveland, M. de Saint Simon, and G. T. Seaborg, Phys. Rev. C **21**, 1783 (1980).
[11] J. Adam, Chitra Bhatia, K. Katovsky *et al.*, Eur. Phys. J. A **47(7)**, 85 (2011).
[12] F. Rahimi, D. Gheysari, G. Remy *et al.*, Phys. Rev. C **8**, 1500 (1973).
[13] C. Damdinsuren, V. Iljushchenko, P. Kozma *et al.*, Yad. Fiz. **52**, 330 (1990).
[14] S. Stoulos, W. Westmeier, R. Hashemi-Nezhad, M. Fragopoulou, A. Lagoyannis, and M. Zamani, Phys. Rev. C **85**, 024612 (2012).
[15] A. R. Balabekyan, N. A. Demekhina, G. S. Karapetyan *et al.*, Phys. Rev. C. **89**, 054604 (2014).
[16] J. Frána, J. Radiol. Nucl. Chem. **257**, 583 (2003).
[17] R. B. Firestone, in *Tables of Isotopes*, 8th ed., update with CD ROM, edited by S. Y. Frank Chu (CD-ROM editor) and C. M. Baglin (Wiley Interscience, New York, 1998).
[18] H. Baba, J. Sanada, H. Araki *et al.*, Nucl. Instrum. Methods A **416**, 301 (1998).
[19] J. Cugnon, C. Volant, and S. Vuillier, Nucl. Phys. A **625**, 729 (1997).
[20] V. S. Barashenkov and V. D. Toneev, *Interactions of High-Energy Particles and Nuclei with Nuclei* (Atomizdat, Moscow, 1972).
[21] H. Kudo, M. Maruyama, M. Tanikawa, T. Shinozuka, and M. Fujioka, Phys. Rev. C **57**, 178 (1998).
[22] C. L. Branquihno and V. J. Robinson, J. Inorg. Nucl. Chem. **39**, 921 (1977).
[23] P. Kozma, J. Kliman, and M. Leonard, Czecj. J. Phys. B **38**, 973 (1988).
[24] K. Summerer and B. Blank, Phys. Rev. C **61**, 034607 (2000).
[25] V. M. Maslov, Nucl. Phys. A **717**, 3 (2003).
[26] M. C. Duijvestijn, A. J. Koning, J. P. M. Beijers, A. Ferrari, M. Gastal, J. van Klinken, and R. W. Ostendorf, Phys. Rev. C **59**, 776 (1999).
[27] C. Chung and J. J. Hogan, Phys. Rev. C **24**, 180 (1981).
[28] D. R. Nethaway and B. Mendoza, Phys. Rev. C **6**, 1827 (1972).
[29] P. Napolitani, K.-H. Schmidt, and L. Tassan-Got, J. Phys. G.: Nucl. Part. Phys. **38**, 115006 (2011).
[30] P. Bonche *et al.*, Nucl. Phys. A **436**, 265 (1985)
[31] E. Bonnet *et al.*, Phys. Rev. Lett. **103**, 072701 (2009).
[32] T. Enqvist, P. Armbruster, J. Benlliure *et al.*, Nucl. Phys. A **703**, 435 (2002).
[33] T. Fukahori, O. Iwamoto, and S. Chiba, in *Proceedings of the Seventh International Conference on Nuclear Criticality Safety, ICNC2003*, JAERI-Conf 2003-019, Parts 1 and 2 (Japan Atomic Energy Research Institute, Tokai-mura, Japan, 2003), p. 144.
[34] H. L. Bradt and B. Peters, Phys. Rev. **77**, 54 (1950).
[35] P. Bondorf, A. S. Botvina, A. S. Iljinov, I. N. Mishustin, and K. Sneppen, Phys. Rep. **257**, 133 (1995).